Indian Journal of Engineering & Materials Sciences
Vol. 30, April 2023, pp. 305-313
DOI: 10.56042/ijems.v30i2.1713

Experimental Investigation on the Synthesis of Al5086-GRN-ηSiC Hybrid Surface Composite using Additive Powder Fed Friction Stir Processing

Gagandeep Singh Raheja[a], Chander Prakash[a]*, & Shankar Sehgal[b]

[a]School of Mechanical Engineering, Lovely Professional University, Phagwara Punjab 144 411, India

[b]Mechanical Engineering, University Institute of Engineering and Technology, Panjab University Chandigarh 160 014, India

Received; 31 December 2021& Accepted 21 March 2022

In the current research work, graphene (GRN) and nano-silicon carbide (SiC) reinforced Al5086-alloy based hybrid surface composites has been developed using a unique surface engineering technique called additive-powder-fed friction stir processing (APF-FSP) process. Herein, the mechanical exfoliation of graphite into GRN has been carried out using APF-FSP process to improve the microstructural and mechanical properties. The microstructure, morphology, and mechanical properties of as-synthesized hybrid Al5086-GRN-ηSiC surface composite has been investigated. Microscopic analysis has been conducted to scientifically ascertain the grain size, crystal structure and surface morphology of APF-FSP zone. The mechanical properties such as hardness and elastic modulus have also been evaluated using nanoindentation and micro-hardness technique. Nano-indentation and micro-pillar testing techniques have been used to assess mechanical properties in terms of hardness, elastic modulus, and compressive strength of as-developed hybrid Al5086-GRN-ηSiC surface composite. The best optimal condition to obtain the defect free structure is 1800 RPM rotational speed and 40 mm/min transverse speed with trapezoidal shape tool pin geometry. The microstructure and morphological examination reveal that the grain size of Al-matrix gets refined from 30 µm to ~8 µm and reinforcements (GRN/ ηSiC) are uniformly distributed in the matrix, which is expected to improve the mechanical properties. The SEM and TEM morphology analysis show that the diphasic nano-mixture cluster of ηSiC and GRN in the range (100-200 nm) have been formed and GRP co-exist in multi-layer of atoms in Al-matrix owing to mechanical exfoliation of graphite. The highest hardness (145 $HV_{0.3}$) and tensile strength (385±5 MPa) have been obtained. Overall, findings of this work conclude that APF-FSP offers up new possibilities for fabricating functionalized surface composites with improves mechanical properties for aerospace and automobile industries.

Keywords: Al5086 alloy, Additive powder fed, Friction stir processing, Surfaces, Composite materials, Hardness

1 Introduction

In the era of modernization, the manufacturing sectors have always sought and developed new multiscale and multifunctional materials with superior quality for higher productivity and efficiency[1, 2]. Aluminium (Al) alloys and composites have been the ultimate choice because of their lightweight, outstanding mechanical, and tribological qualities[3–6]. The desired properties of Al-based alloys and composites have been tailored by processing its microstructure and appropriate reinforcements[7, 8]. There are several methods reported for the synthesis of Al-based alloys and composites, such as stir casting[9], powder metallurgy[10], spark plasma sintering[11,12], microwave sintering[13], and solid-state methods[14]. But these methods have several limitations, such as microstructural defects, cracks, porosities, insulation, agglomeration, and unavoidable interfacial reaction that reduced the mechanical properties of as developed composites[15,16]. Secondary treatment methods have been applied to remove these defects via plastic deformation[17–19]. Friction stir processing (FSP) has drawn the most interest from researchers among various plastic deformation and microstructural modification techniques, owing to its outstanding solid-state and eco-friendly processing[20, 21].

Several researchers have developed different AMCs using the FSP process with reinforcement particles SiC, Al2O3, ZrB2, TiO2, TiC, and B4C[22–28]. The reinforcement of ZrB2 into Al2024-matrix has been used in improving microstructure and inducing super plasticity[29].The plasticity increasesto 92.5% as compared to the base substrate. Yuvaraj *et al.* have developed Al5083/B4C surface composite using the FSP process and studied the microstructural properties, mechanical property, and tribological performance[30]. The results show that the as developed

*Corresponding author (E-mail: chander.mechengg@gmail.com)

Al5083/B4C surface composite exhibits fine grain; due to which, the mechanical property increases. Jeon *et al.*[31] have investigated the effect of graphene in the form of GO/water colloid in Al5052-matrix on the thermal conductivity and mechanical properties. It has been reported that thermal conductivity increases by 15%, and excellent mechanical properties are obtained. Rajeshkumar *et al.*[32] have developed Al/Gr surface composite using the FSP process and have reported that ultrafine grain structure is obtained after ultrasonic treatment followed by the FSP process. Kumar *et al.*[33] have developed Al-based surface composite using industrial waste (fly ash and red mud) as reinforcements using the FSP process. The mechanical and tribological performance of as-developed composites have also been compared. The presence of fly ash and red mud reinforcement in Al-matrix has improved the mechanical and wear resistance properties and has proved a potential choice compared to costlier reinforcements. Sharma *et al.*[34] have synthesized Al6061-SiC-graphite hybrid surface composites using FSP and studied the effect of rotational speed on the mechanical properties. It has been observed that the rotation speed significantly affects mechanical performance. At 2200 RPM, the FSP processed Al6061-SiC-graphite hybrid surface composites possess high mechanical properties as compared with the composites developed at 2500 RPM. Furthermore, Sharma *et al.*[35] have compared the microstructural characteristics, mechanical properties, and wear resistance of Al-SiC (graphene, graphite, and CNT) composites developed by FSP. Among all developed composite groups, Al-SiC-GNP exhibit excellent mechanical and tribological properties. FSP has recently been used to synthesize graphene-reinforced AMC with improved properties[36]. The graphene has been in-situ produced in Al-matrix by direct exfoliation of graphite owing to the dynamic stirring of friction tool and has increased the properties of as-developed composite[37]. However, it's still unclear whether FSP causes graphene to exfoliate in situ with other micro/nano-scale reinforcements.

From the available literature, it can be seen that the FSP technique is suitable for all types of ceramic reinforcement material. However, very limited research is available on nano-SiC and graphene reinforcement combinations. In this paper, a newly developed surface engineering technique named additive powder fed friction stir processing (APF-FSP) has been explored to exfoliate in situ graphene from nano-scale graphite and SiC. A detailed microstructural characterization, mechanical properties analysis, and tribological properties have been studied.

2 Materials and Methods

The additive powder fed friction stir processing (APF-FSP), an innovative surface engineering technique, was proposed to be used for the synthesis of graphene (GRN) and nano-silicon carbide (ηSiC) reinforced Al-alloy based hybrid surface composite. Al5086 alloy plate of dimensions 110 × 50 × 5 mm^3 was used as the workpiece. Figure 1 shows the experimental setup of in-house developed APF-FSP using a vertical milling machine with a maximum

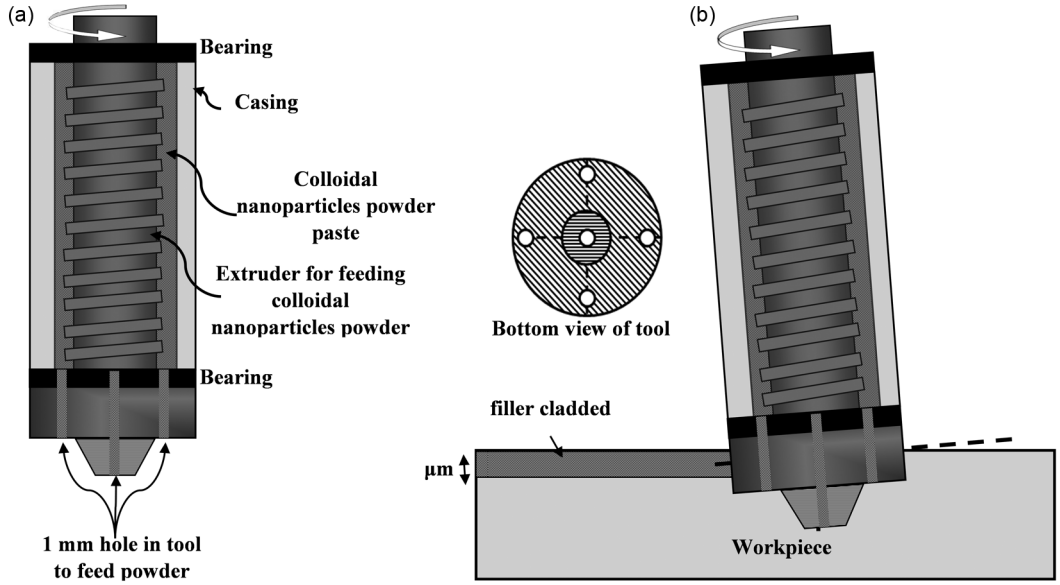

Fig. 1 — (a) Tool geometry, and (b) Additive powder fed friction stir processing (APF-FSP).

motor capacity of 3.7 kW. The APF-FSP comprised two systems, including screw extruder and tool, refer to Fig. 1(a). The screw extruder rotates at the same speed as the tool and exerts hydrostatic pressure which feeds the colloidal nanoparticle paste of graphite and ηSiC in the Al5086 alloy matrix refer Fig. 1(b). For friction processing, a special design tool was fabricated from tungsten carbide materials, which comprised threads that increased the materials flow due to plastic deformation during processing and a micro-sized drilled hole (0.8 mm) for injecting colloidal nanoparticle paste. The length of the pin was 3 mm, and the 16 mm shoulder diameter had a 2º concave angle.

Figure 2 shows the actual photograph of the experimental APF-FSP setup. The colloidal paste was prepared by mixing GRN (10-50 nm) nanoparticles and ηSiC (~25 nm) in a 1:1 ratio by dispersing in water/ethanol. Figure 3 shows the SEM micrograph of graphite and ηSiC. The APF-FSP experiments were carried out by varying the traversal speed (30 and 40 mm/min) at rotational speed (1200 and 1800 RPM). The dimensions of backing plates and fixtures were chosen as per the length and width of the milling machine table. Vertical clamping pressures were used with pressure bars to prevent plates from lifting and also to provide uniform temperature distribution across the plates. Two L-shaped mild steel plates were utilized to avoid the discretion of two plates and also to provide side pressure on the workpieces during welding, with two end-screwed bolts on each plate. The width of the backing plate was made somewhat smaller than the entire width of the two plates to be processed for direct lateral pressure on specimens. All experiment sets were subjected to microstructural characterization and mechanical testing because the integrated parameters resulted in defect-free weld connections with reliable joint strength. Figure 4 shows the detailed methodology for the development of surface composite and its characterization.

For microstructural examination, the samples of dimension (35×10 ×5 mm) were cut from APF-FSP processed zone. The samples were polished with emery papers (600-2000 grit) and diamond paste followed by etching with Kellers' solution (nitric acid 7.5 ml, hydrochloric acid 22.5 ml, hydrofluoric acid 7.5 ml and distilled water 12.5 ml) for 10 seconds. The microstructural characterization was done with optical microscopy (OM), scanning electron microscopy (SEM) and energy-dispersive X-ray spectroscopy (EDS) as pre procedure reported in previous studies[38–40]. Vickers microhardness was measured using a microhardness tester across the centre line of each sample by setting indentation time

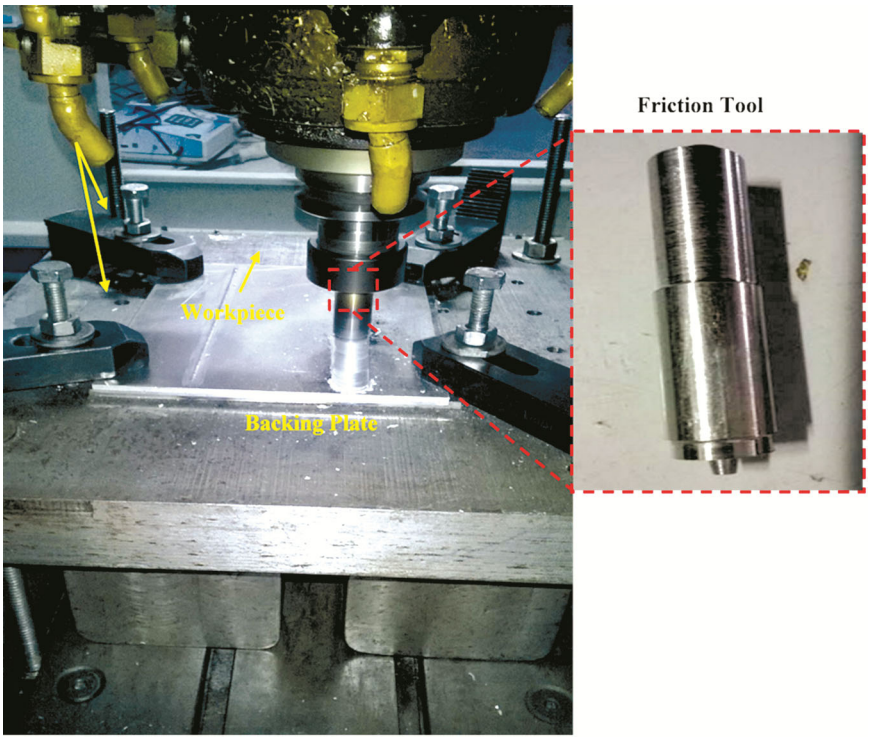

Fig. 2 — Experimental set-up of Additive powder fed friction stir processing (APF-FSP).

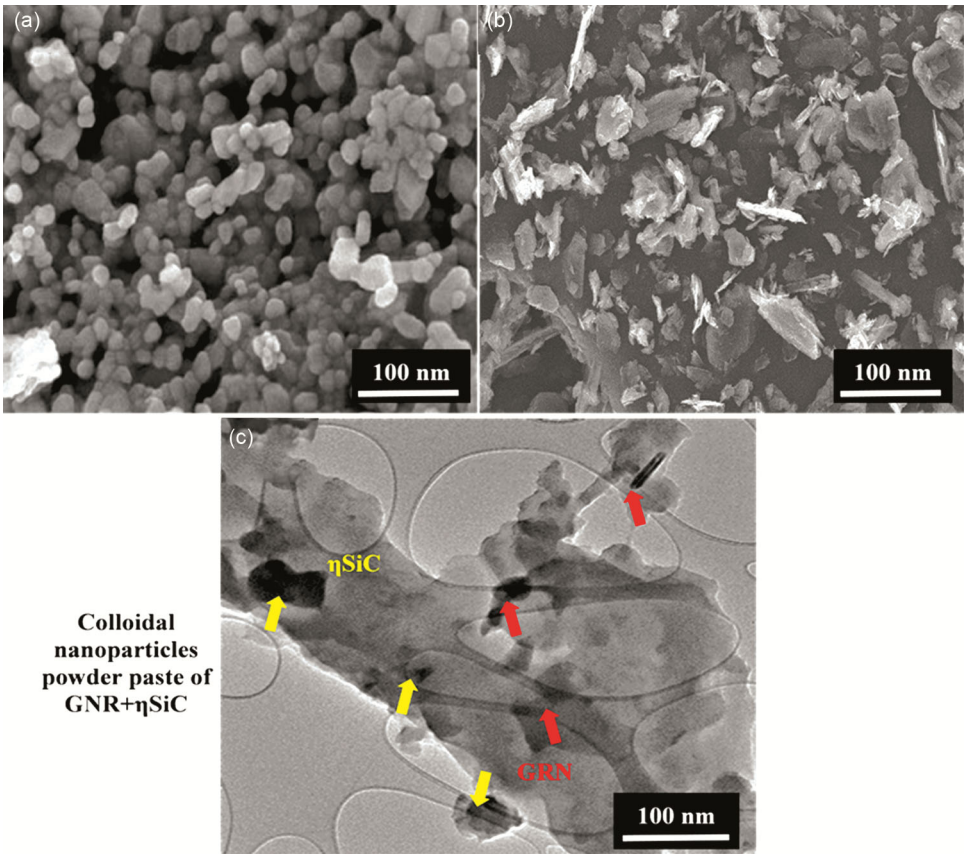

Fig. 3 — SEM and TEM image of powders: (a) Nano-SiC, (b) graphite, and (c) colloidal nano-particle paste of graphite and ηSiC.

to 10 s for each indent while maintaining 0.5 mm interval and applied load of 100 gf[41].

The micro-mechanical behaviour was measured in terms of hardness and elastic modulus of as-developed Al5086-GRN-ηSiC hybrid composite using nanoindentation system (PI-88 nanoindenter, Hysitron Inc., USA with diamond Berkovich tip) at indentation load of 1 mN together with loading/unloading rates of 0.5 mN/s[2, 42]. The compressive strength of as-developed Al5086-GRN-ηSiC hybrid composite was found via micro-pillar testing using a nanoindentation system. An SEM incorporated with Ga+ focused beam (FIB-SEM) was employed to fabricate the micro-pillars. To ensure that the indenter does not touch the sample surface, except the micro-pillars in the course of compression, a sufficient void was kept (30 µm) between the micro-pillar and surrounding materials. At first, the milling pattern was executed at a relatively higher current. The indenter tip was swapped with a 5 µm diameter flat diamond on the same nanoindentation system for in-situ compression test. During in-situ compression, loading and unloading rates were 3 and 50 nm/s respectively,

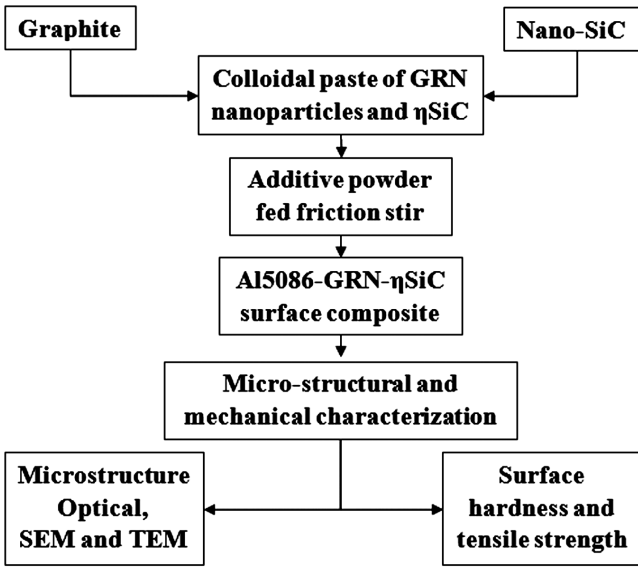

Fig. 4 — Detailed methodology of surface composite development and characterization.

where the loading rate was equivalent to 10-3 s-1 strain rate. The load-displacement graphs were recorded together with the corresponding video of the compression. According to the method reported by

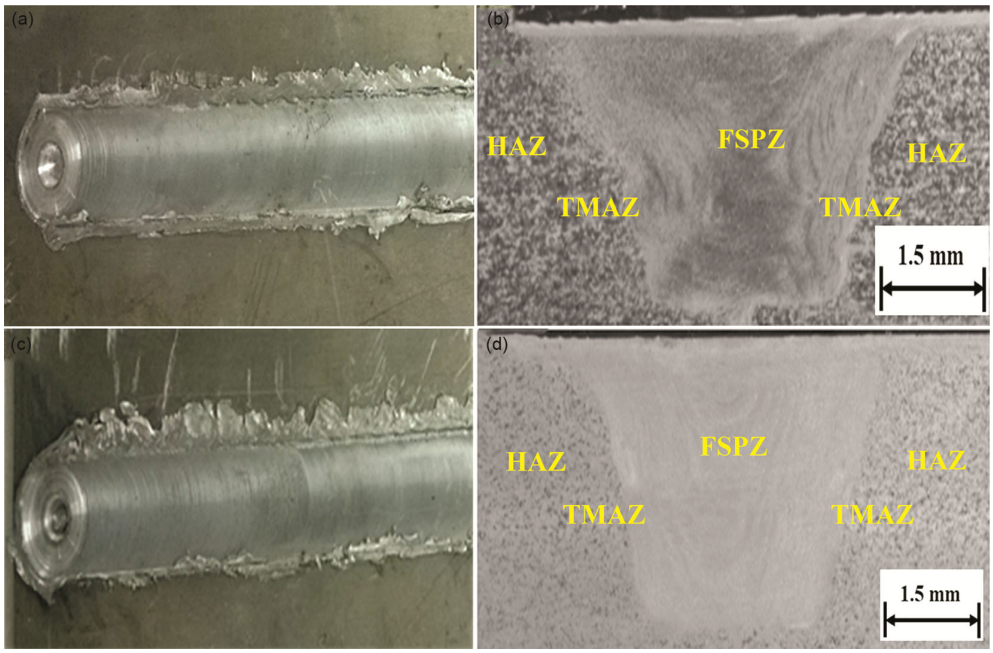

Fig. 5 — Macrograph of FSP processed zone under different speed: (a-b) 1200 RPM and (b) 1800 RPM.

Basak *et al.*[2], the load-displacement curves were converted to stress-strain curves.

3 Results and discussion

Figure 5 shows the cross-section macrograph of the FSP processed zone with different transverse speeds (30 and 40 mm/min) and rotational speed (1200 and 1800 RPM). Friction stir processing zone (FSPZ), thermomechanical affected zone (TMAZ), and heat-affected zone (HAZ) were identified in the macrograph. From the macrograph, it can be seen that the Al5086-GRN-ηSiC hybrid composite was defect-free and sound. Numerous onion rings appear in the stir zone, which comprises different lamellar structures generated due to dynamic stirring of tool pin, and it occurs excess in processing. In the literature, similar results were reported: the emergence of onion rings in FSPZ due to materials flow induced by the plastic deformation produced by tool pin geometry and stirring action[30]. Flash generally forms because of excessive heat produced owing to the high rotational and low transverse speed[37]. FSP process tends to produce surface flash since the tool shoulder is obliged to penetrate below the workpiece surface, and the processing is associated with heat generation and mechanical mixing. Generally, excess materials occur during the process of flashing out, but some materials somehow tend to get stuck on the processed surface. These

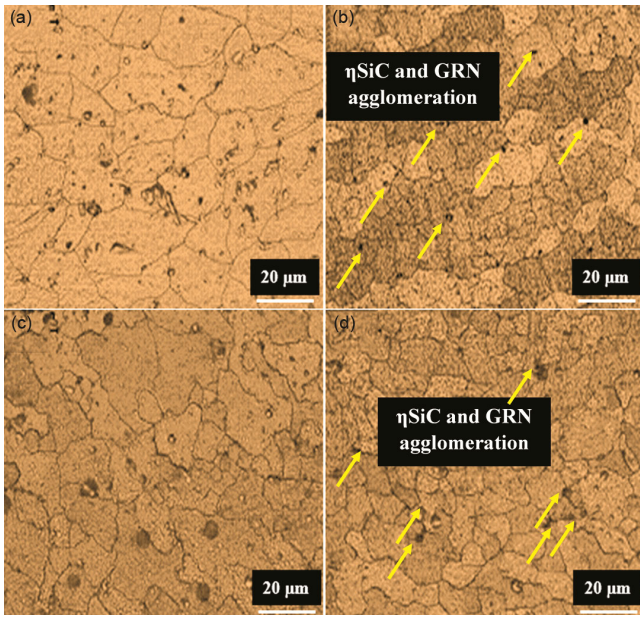

Fig. 6 — Microstructure of heat affected zone (HAZ) and friction stir processed zone (FSPZ) at 1200rpm speed with (a) 30 mm/min and (b) 40 mm/min.

flashes could be eliminated by machining the processed plate's top and bottom surfaces. The microstructure of materials determines the mechanical properties.

Figure 6 shows the microstructure of heat affected zone (HAZ) and friction stir processed zone (FSPZ) at 1200rpm speed with 30mm/min and 40 feed. At 30 mm/min feed, it can be seen that HAZ has a coarse

grain size in the range of 20-25 µm (refer Fig. 6a), whereas FSPZ comprised grain size in the range of 13-15 µm (refer Fig. 6b). This is attributed to the fact that in the FSPZ region, the grains of Al-matrix were re-arranged and recrystalized due to plastic deformation induced by the tool. From the micrograph, the nano-homogenous distribution of ηSiC can be clearly seen in the Al-matrix, owing to limited metal flow and low plasticity at low speed (1200 RPM). However, the GRN layer was homogeneously and uniformly distributed and entered up to certain micrometres in Al-matrix. The uniform graphene film was developed due to the shearing of particles developed by friction tool near the subsurface regions where subsurface strains are extremely high. With the increase in feed (transverse speed), a significant change in the microstructure was observed. At 40 mm/min feed, it can be seen that HAZ has a coarse grain size in the range of 18-22 µm (refer Fig. 6c), whereas FSPZ comprised grain size in the range of 10-12 µm (refer Fig. 6d). With the increase in transverse speed, the plasticized metal flow increased; as a result, finer grain growth occurred in the Al-matrix, and a more uniform distribution of reinforcement particles occurred.

Figure 7 shows the HAZ and FSPZ microstructure at 1800rpm speed with 30mm/min and 40 feed. Similarly, the HAZ region comprised coarse gain and FSPZ comprised fine grain structure; however, the grain size in HAZ and FSPZ is smaller than the microstructure obtained at 1200 RPM. At 30 mm/min feed, it can be seen that HAZ has a coarse grain size in the range of 20-22 µm (refer Fig. 7a), whereas FSPZ comprised grain size in the range of 8-10 µm (refer Fig. 7b). It can be seen that ηSiC and GRN were homogeneously and uniformly distributed. The dark grey patches correspond to the GRN layer, and ηSiC is reinforced and deposited in the Al-matrix. This is attributed to high materials flow and plastic deformation due to heat generated during high rotation speed. With the increase in feed (transverse speed), the grain structure was further recrystallized, and finer grain growth was obtained. At 40 mm/min feed, it can be seen that HAZ has a coarse grain size in the range of 12-15 µm (refer Fig. 7c), whereas FSPZ comprised grain size in the range of 6-8 µm (refer Fig. 7d). The yellow arrow and circles correspond to the distribution of ηSiC and GRN particles, respectively; owing to low density, the GRN particles float on the surface. Due to high speed, a large amount of heat is generated, which causes more plastic low of material. As a result, strain increased in the region where GRP is present, and film squeezed out the form and floated on the top surface. This results in an improvement in mechanical properties.

Figure 8 presents the SEM-micrograph, EDS-spectrum, and TEM-mage of base Al5086 alloy and APF-FSP developed Al5086-GRN-ηSiC hybrid composite. The unprocessed base Al5086 alloy compromised plan surface morphology. EDS spectrum

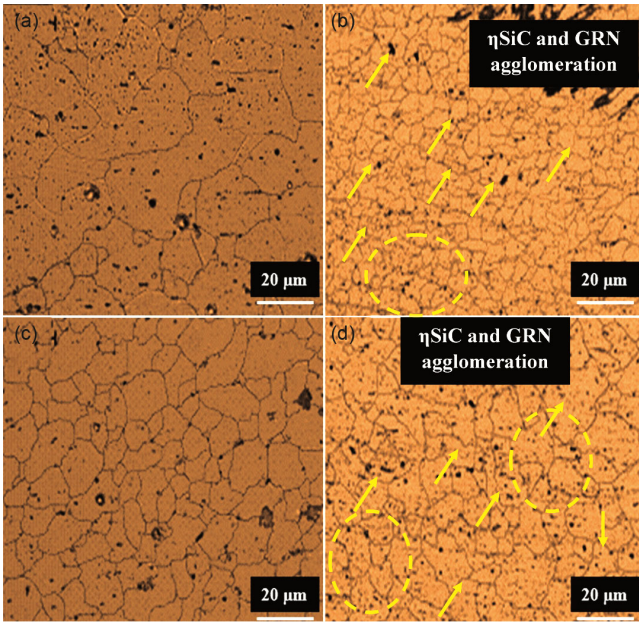

Fig. 7 — Microstructure of heat affected zone (HAZ) and friction stir processed zone (FSPZ) at 1800rpm speed with (a) 30mm/min, and (b) 40 mm/min feed.

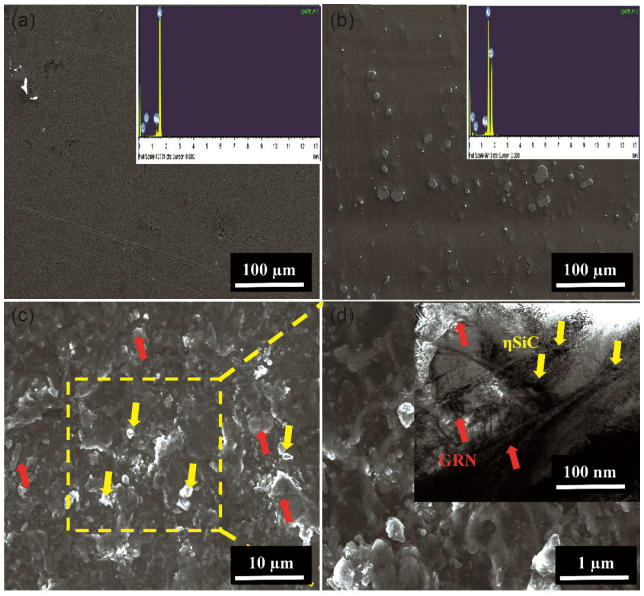

Fig. 8 — EDS and SEM-micrograph of (a) Al5086 alloy, (b) Al5086-GRN-ηSiC hybrid composite, (c) SEM-micrograph (2500 ×), and (d) SEM micrograph (10000 ×) and TEM micrograph.

confirmed the presence of Al, Mg, C, and O elements, which further conferred the elemental composition of the base alloy (refer Fig. 8a). The agglomeration GRN and ηSiC can be observed in the APF-FSP developed Al5086-GRN-ηSiC hybrid composite (at 1800 RPM and 40 mm/min) and associated EDS-spectrum confirm the Si and C peak along with Al peaks (refer Fig. 8b). The agglomeration GRN and ηSiC can be seen in the Al-matrix in the form of large clusters. During APF-FSP processing, the graphite powder was exposed to high material flow due to plastic deformation induced by stirring action, resulting in a large amount of graphene exfoliated in thin films from graphene (refer Fig. 8c). The dark/bright-field diphasic nano-mixture cluster of ηSiC and GRN in the range (100-200 nm) can be seen in SEM and TEM-micrograph, refer Fig. 8(d). The GRN co-exist in multi-layer of atoms in Al-matrix due to graphite's mechanical exfoliation. No visible defects, cracks, and impurities formed at the carbon-to-aluminium interface.

Figure 9 shows the XRD pattern of un-processed Al5086 alloy and FSP-developed Al5086-GRN-ηSiC hybrid composite at RS; 1800 and F:40 mm/min. It can be seen that the un-processed Al5086 alloy comprised only Al, Mg, and Cu-peaks. Different intensities of the peak were noticed at diffraction angles (2θ). Similarly, the intensity of these peaks was observed to be low in the un-processed Al5086 alloy higher in the FSP-developed Al5086-GRN-ηSiC hybrid composite developed. Graphene, Al, SiC peaks can be seen in the FSP-developed Al5086-GRN-ηSiC hybrid composite. The intensity of (200) peak for FSP-developed Al5086-GRN-ηSiC hybrid composite corresponding to aluminum which has FCC crystal structure, was observed significantly higher is an indication of texture effect caused due to stirring action in the thermo-mechanically affected zone. The close-packed planes (111) in HCP metals and (200) in FCC metals are the highest density planes that serve an important role in material properties. The FSP-developed Al5086-GRN-ηSiC hybrid composite consists of a higher fraction of FCC metal that excellently enhances a joint's mechanical properties and mechanical properties.

Figure 10 shows the microhardness profile of Al5086-GRN-ηSiC hybrid composite processed at different rotational speeds and feed. The hardness measurements were recorded across the center of the joint cross-section using a Vickers microhardness testing machine. The hardness values of all the processed zone revealed asymmetry along the weld length due to the high temperature generated in the SZ and improper heat dissipated into the adjoining material during the processing zone. The low hardness values are noticed in TMAZ on the advancing side where the fracture occurred, and the

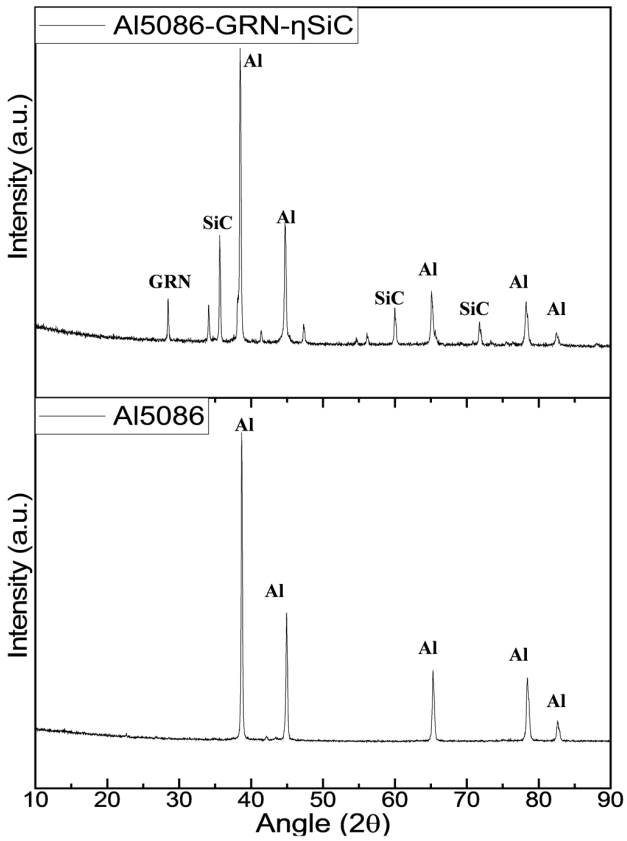

Fig. 9 — XRD patterns for un-processed Al-5086 and FSP-developed Al5086-GRN-ηSiC hybrid composite.

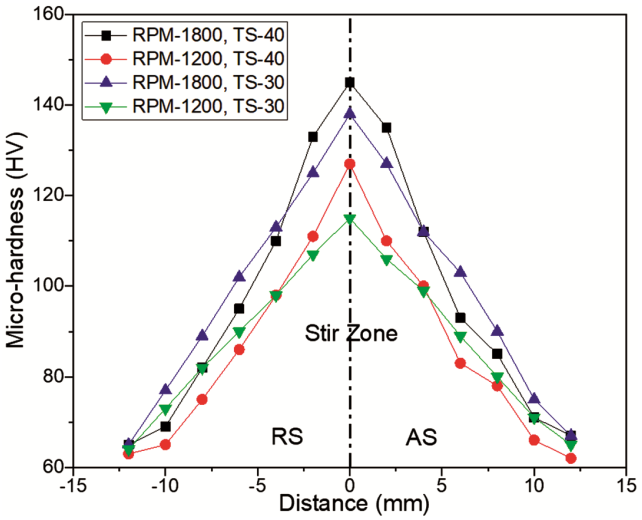

Fig. 10 — Vickers microhardness profile across the Al5086-GRN-ηSiC hybrid composite at different rotational and transverse speed.

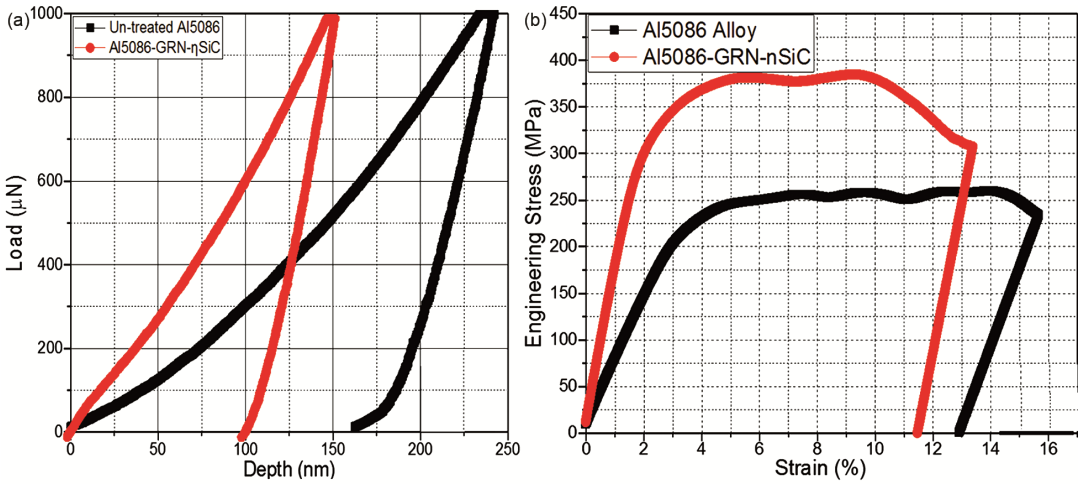

Fig. 11 — Micro-mechanical behavior in terms of (a) elastic modulus, and (b) compressive strength of un-treated Al-5085 alloy and FSP-developed Al5086-GRN-ηSiC hybrid composite.

lowest value of 62 HV is observed for a zone obtained with 30 mm/min transverse speed and 1200 rpm spindle speed. The Al5086-GRN-ηSiC hybrid composite developed with RS: 1800 rpm and 40 mm/min transverse speed produced the highest hardness value of 145 HV in SZ adjacent to the thermo-mechanically affected zone on the retreating side. This could be the consequential reason for the higher ultimate tensile strength of the joint fabricated with these parameters. The small particles of the intermetallic compound and fine grains in the stir zone are the key reason for improved hardness values in the SZ because grain size refinement has a significant role in material robustness.

The micromechanical behaviour of un-treated Al5086 alloy and FSP-developed Al5086-GRN-ηSiC hybrid composite was investigated in terms of elastic modulus and compressive strength using a nanoindentation system. Figure 11(a) shows the loading/unloading indentation curve, which indicates that the materials showed both elastic and plastic deformation, with some elastic recovery after full unloading. The elastic modulus was determined using the Oliver–Pharr method. The slope of the FSP-developed Al5086-GRN-ηSiC hybrid composite was less than that of the un-treated Al5086 alloy. This is attributed because the top layer of Al5086-GRN-ηSiC hybrid composite comprised fine grain structure, which exhibits high hardness. Correspondingly, the Al5086-GRN-ηSiC hybrid surface composite samples possessed a high elastic modulus (172 GPa) compared to the un-treated Al5086 alloy (75 GPa). Figure 11(b) shows the stress-strain curves of the micro-pillars as converted from associated load-displacement curves of un-treated Al5086 alloy and FSP-developed Al5086-GRN-ηSiC hybrid composite. The graph shows that the stress-strain behaviour of the Al5086-GRN-ηSiC hybrid composite is distinct from the un-treated Al5086 alloy. The Al5086-GRN-SiC hybrid composite's top surface layer shows to be able to withstand more stress than the untreated Al5086 alloy, but it is unable to assimilate strain. It is no wonder, given that the Al5086-GRN-SiC hybrid composite is hard and brittle when compared to untreated Al5086 alloy, as evidenced by nanoindentation data. The micro-pillars on the top surface layer of the Al5086-GRN-SiC hybrid composite break down (collapse) completely within less than 12% of strain, as evidenced by the videos taken during the micro-pillar compression tests. The Al5086-GRN-ηSiC hybrid composite offered high ultimate strength (385 MPa). Compared to that, stress-strain curves of un-treated Al5086 alloy appear to sustain considerably more strain (up to 15 %). The un-treated Al5086 alloy sample offered high ultimate strength (255 MPa).

4 Conclusion

In the present research work, Al5086-GRN-ηSiC hybrid surface composite has been developed using the friction stir processing technique. Following conclusions can be drawn from this research work:

- The rotation speed (1800 RPM) and feed/transverse speed (40 mm/min) are the best optimal conditions to synthesize the best quality and defect-free Al5086-GRN-ηSiC hybrid surface composite.

- The GRN and ηSiC reinforcements are homogeneously distributed in the Al-matrix. The grain size has been drastically reduced in the processed zone from 23 to 6 μm.
- The SEM and TEM morphology analysis reveal that the diphasic nano-mixture cluster of ηSiC and GRN in the range (100-200 nm) are formed.
- HR-TEM investigation shows that GRP co-exists in multi-layer of atoms in Al-matrix owing to mechanical exfoliation of graphite, which improves the mechanical properties of the composite.
- Al5086-GRN-ηSiC hybrid surface composite exhibit hardness (145 HV), tensile strength (385 MPa), and elastic modulus (172 GPa). Apart from this, a dense, light weight, and high strength Al5086-GRN-ηSiC hybrid surface composite has been developed.
- As developed Al5086-GRN-ηSiC hybrid surface composite can offer high wear resistance and tribological properties.
- The future extension of the research study will cover the tribological performance of as developed Al5086-GRN-ηSiC hybrid surface composite.

References

1 Buchta M, Kiesswetter BE, Schaper BM, Zschiesche CW, Schaller DKH, Kuhlmann AA & Letzel AS, *Environ ToxicolPharmacol*, 19 (2005) 677.
2 Yang Y, Song X, Li X, Chen Z, Zhou C, Zhou Q & Chen Y, *Adv Mater*, 30 (2018) 1.
3 Basak AK, Pramanik A & Prakash C, *Mater Sci Eng A*, 763 (2019) 138141.
4 Xie Y, Meng X, Mao D, Qin Z, Wan L& Huang Y, *ACS Appl Mater Interfaces*, 13 (2021) 32161.
5 Zhu J, Jiang W, Li G, Guan F, Yu Y& Fan Z, *J Mater Process Technol*, 283 (2020) 116699.
6 Chen F, Gupta N, Behera RK & Rohatgi PK, *Jom*, 70 (2018) 837.
7 Mavhungu ST, Akinlabi ET, Onitiri MA &Varachia FM, *Procedia Manuf*, 7 (2017) 178.
8 Zhang K, Jang H & Le Q, *J Compos Compd*, 2 (2020) 76–84.
9 Wang P Eckert J, Prashanth KG, Wu MW, Kaban I, Xi LX & Scudino S, *Trans Nonferrous Met Soc China*, 30 (2020) 2001.
10 Sahu MK & Sahu RK, in *Advanced casting technologies*, edited by Vijayaram T (IntechOpen, London), 2018, 111.
11 Chamroune N, Mereib D, Delange F, Caillault N, Lu Y, Grosseau-Poussard JL & Silvain JF, *J Mater Sci*, 53 (2018) 8180.
12 Ghasali E, Alizadeh M, Shirvanimoghaddam K, Mirzajany R, Niazmand M, Faeghi-Nia A & Ebadzadeh T, *Mater Chem Phys*, 212 (2018) 252.
13 Prakash C, Singh S, Sharma S, Garg H, Singh J, Kumar H & Singh G, *Mater Today Proc*, 21 (2020) 1637.
14 Askarnia R, Ghasemi B, Fardi SR, Lashgari HR & Adabifiroozjaei E, *Adv Compos Mater*, 30 (2021) 271.
15 Abbas AT, Pimenov DY, Erdakov IN, Taha MA, El Rayes MM & Soliman MS, *Metals (Basel),* 8 (2018) 394.
16 Khodabakhshi F &Gerlich AP, *J Manuf Process*, 36 (2018) 77.
17 Chak V, Chattopadhyay H & Dora TL, *J Manuf Process*, 56 (2020) 1059.
18 Kumar R, Ranjan N, Kumar V, Kumar R, Chohan JS, Yadav A, Sharma S, Prakash C, Singh S & Li C, J *Mater Eng Perform*, 31 (2022) 2391.
19 Raheja GS, Singh S & Prakash C, *Mater Today Proc*, 50 (2021) 539.
20 Węglowski MS, *Arch Civ Mech Eng*, 18 (2018) 114.
21 Patel V, Li W, Vairis A &Badheka V, *Crit Rev Solid State Mater Sci*, 44 (2019) 378.
22 Sudhakar M, Srinivasa Rao CH & Saheb KM, *Mater Today Proc*, 5 (2018) 929.
23 Li K, Liu X & Zhao Y, *Coatings*, 9 (2019) 129.
24 Butola R, Tyagi L, Singari RM, Murtaza Q, Kumar H & Nayak D, *Mater Res Express*, 8 (2021) 016520.
25 Jayaseelan P, Christy T V., Prabhu Rubesh G & Srinivasan R, *J Comput Theor Nanosci*, 16 (2019) 719.
26 Kumar S, Kumar K, Maurya M & Vishal, *Int J Mater Res*, 112 (2021) 898.
27 Odhiambo JO, Yoshida M, Otsu A, Yi LF, Onda T & Chen ZC, *J Compos Mater*, 56 (2022) 1987.
28 Veeresh Kumar GB, Pramod R, Hari Kiran Reddy R, Ramu P, Kunaal Kumar B, Madhukar P, Chavali M, Mohammad F & Khiste SK, *Nanomaterials*, 11 (2021) 1.
29 Zhao Y, Kai X, Chen G, Lin W & Wang C, *Prog Nat Sci Mater Int*, 26 (2016) 69.
30 Yuvaraj N, Aravindan S & Vipin, *J Mater Res Technol*, 4 (2015) 398.
31 Jeon CH, Jeong YH, Seo JJ, Tien HN, Hong ST, Yum YJ, Hur SH & Lee KJ, *Int J Precis Eng Manuf*, 15 (2014) 1235.
32 Rajeshkumar R, Udhayabanu V, Srinivasan A & Ravi KR, *J Alloys Compd*, 726 (2017) 358.
33 Kumar H, Prasad R, Kumar P, Tewari SP & Singh JK, *J Alloys Compd*, 831 (2020) 154832.
34 Sharma A, Sharma VM, Mewar S, Pal SK & Paul J, *Mater Manuf Process*, 33 (2018) 795.
35 Sharma A, Narsimhachary D, Sharma VM, Sahoo B & Paul J, *Surf Coatings Technol*, 368 (2019) 175.
36 Pradeep S, Jain VKS, Muthukumaran S & Kumar R, *Mater Lett*, 288 (2021) 129382.
37 Liu Y, Chen G, Zhang H, Yang C, Zhang S, Liu Q, Zhou M& Shi Q, *Mater Lett*, 301 (2021) 130280.
38 Prakash C, Singh S, Pabla BS, Sidhu SS & Uddin MS, *Mater Manuf Process*, 34 (2019) 357.
39 Pramanik A, Basak AK & Prakash C, *Heliyon*, 5 (2019) e01473.
40 Singh H, Prakash C & Singh S, *J Bionic Eng*, 17 (2020) 1029.
41 Basak A, Pramanik A, Prakash C & Kotecha K, *Mater Lett*, 305 (2021) 130769.
42 Prakash C, Kansal HK, Pabla BS & Puri S, *J Comput Inf Sci Eng*, 16 (2016) 1.